Monthly Notices of the ROYAL ASTRONOMICAL SOCIETY

MNRAS **538,** L89–L93 (2025) https://doi.org/10.1093/mnrasl/slaf015
Advance Access publication 2025 February 5

Mining the time axis with TRON – II. MeerKAT detects a stellar radio flare from a distant RS CVn candidate

O. M. Smirnov [1,2,3★] A. Golden,[4] T. Myburgh,[1] B. Ngcebetsha,[2,1] C. Tasse,[5,1] I. Heywood,[6,7,1,2] A. J. T. Ramaila,[1,2] M. A. Thompson,[8] J. S. Kenyon,[1] S. J. Perkins,[2] J. Dawson,[1,2] H. L. Bester,[2,1] J. S. Bright,[6,7] N. Oozeer,[2,1] V. G. G. Samboco,[1] I. Sihlangu[2,1] and C. Choza[6,7]

[1]*Centre for Radio Astronomy Techniques and Technologies (RATT), Department of Physics and Electronics, Rhodes University, Makhanda 6140, South Africa*
[2]*South African Radio Astronomy Observatory, Cape Town 7700, South Africa*
[3]*Institute for Radioastronomy, National Institute of Astrophysics (INAF IRA), Via Gobetti 101, I-40129 Bologna, Italy*
[4]*Physics, School of Natural Sciences, Ollscoil na Gaillimhe, University of Galway, University Road, Galway H91 TK33, Ireland*
[5]*GEPI & ORN, Observatoire de Paris, Université PSL, CNRS, 5 Place Jules Janssen, F-92190 Meudon, France*
[6]*Astrophysics, Department of Physics, University of Oxford, Keble Road, Oxford OX1 3RH, UK*
[7]*Breakthrough Listen, Astrophysics, Department of Physics, The University of Oxford, Keble Road, Oxford OX1 3RH, UK*
[8]*School of Physics and Astronomy, University of Leeds, Woodhouse Lane, Leeds LS2 9JT, UK*

Accepted 2025 January 31. Received 2025 January 31; in original form 2024 November 7

ABSTRACT

Medium-time-scale (minutes to hours) radio transients are a relatively unexplored population. The wide field-of-view and high instantaneous sensitivity of instruments such as MeerKAT provides an opportunity to probe this class of sources, using image-plane detection techniques. The previous letter in this series describes our project and associated Transient Radio Observations for Newbies (TRON) pipeline designed to mine archival MeerKAT data for transient and variable sources. In this letter, we report on a new transient, a radio flare, associated with *Gaia* DR3 6865945581361480448, a G type star, whose parallax places it at a distance of 1330 pc. Its duration and high degree of circular polarization suggests electron cyclotron maser instability as the mechanism, consistent with an RS CVn variable.

Key words: methods: data analysis – techniques: interferometric – stars – radio continuum: transients.

1 INTRODUCTION

MeerKAT's high instantaneous sensitivity and large field of view make it an excellent instrument for detecting radio transients. The first letter of this series[1] (Smirnov et al. 2025) introduced our project of mining archival MeerKAT data for new transients and variables using high time cadence interferometric imaging, briefly discussed the Transient Radio Observations for Newbies (TRON) pipeline developed for this project, and reported initial detections of millisecond pulsars in globular clusters.

In this letter, we report on a new transient source detected by TRON. The source has a clear stellar origin. The detection was made in a single pointing that was part of the ``pulsar with anomalous refraction recurring on odd time-scales'' (PARROT) transient follow-up (Smirnov et al. 2024), thus making for two completely unrelated (and astrophysically very different) transient detections in a single MeerKAT observation, which underscores the opening point of our introduction.

2 OBSERVATIONS AND DATA REDUCTION

The observation reported on here were conducted by MeerKAT in conventional synthesis imaging mode, using the *L*-band (856–1712 MHz) and UHF (544–1088 MHz) systems in 4096 channel correlator mode, with 8 s integrations.

The detection observation was a 10-h *L*-band track taken on 2021 June 20, consisting of conventional tracking scans on target, interspersed with shorter scans on a bandpass and gain calibrator. Details of all observations are given in Smirnov et al. (2024); this particular epoch is referred to as 'L2' therein. Other observations reported on here were structured similarly, using a mix of *L*-band and UHF systems.

2.1 Data reduction

As highlighted in the first letter of this series, the inputs to TRON are, generally, yielded by any conventional calibration and imaging workflow. All that is required is a set of calibrated visibilities, and a deep sky model. For the PARROT observations, we used the calibration pipeline described by Smirnov et al. (2024). The corrected data and model image from the pipeline was then passed through TRON, as described in Letter I (Smirnov et al. 2025).

★ E-mail: o.smirnov@ru.ac.za
[1]https://arxiv.org/abs/2501.09488

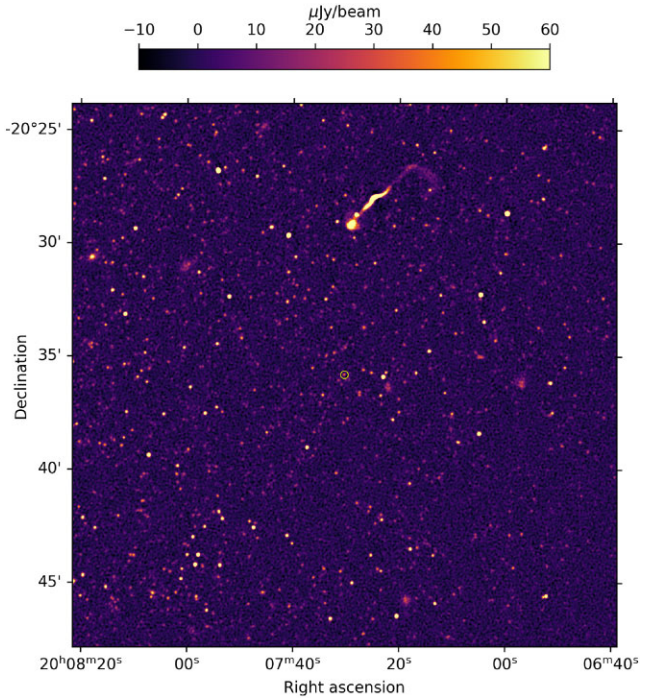

Figure 1. MeerKAT image of the field surrounding *Gaia* DR3 6865945581361480448 at 1.28 GHz. The position of the star is marked by a circle.

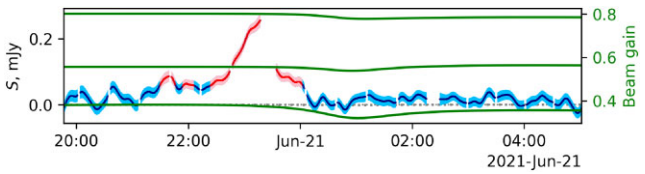

Figure 2. Full *L* band, 240 s-smoothed light curve of *Gaia* DR3 6865945581361480448. Units are apparent flux. Time is UTC. Error bars (computed as the local image rms) are plotted in a lighter shade. 4σ deviations are indicated with a different shade. The three curves (refer to the right *y* axis for scale) show the power beam gain in the direction of the source as a function of time for the bottom (highest gain), mid, and top (lowest gain) end of the band.

3 RESULTS

The PARROT L2 epoch was processed with sole intent of validating TRON on a known variable source, i.e. the PARROT itself. While the PARROT was reliably detected (at time-scales of 15 s and longer), the reprocessing yielded a second transient discovery, MKT J200730.4−203550, detected at time-scales of 30 s and longer (Figs 1, and 2). The fitted FK5 position of the radio source is $\alpha = 20^{\rm h}07^{\rm m}30\overset{\rm s}{.}41(1), \delta = -20^{\circ}35'49\overset{''}{.}6(2)$. This matches to within 1.5 arcsec the position of *Gaia* DR3 6865945581361480448 (Gaia Collaboration 2016, 2023).

We can estimate the probability of a false-positive association by estimating the local density of *Gaia* sources. *Gaia* contains 82522 sources within a circular $r = 1^{\circ}$ aperture centred on the source position, giving an average source density of 259251 deg^{-2}. This translates to 0.014 sources per a $r = 1.5$ arcsec aperture, or a false-positive rate of 1.4 per cent. We note that arcsec-level astrometric offsets in MeerKAT radio positions are not unusual (e.g. Heywood et al. 2022), and are most likely driven by uncertainties in the gain calibrator and the correlator geometric model.

Table 1. Full-band flux measurements for *Gaia* DR3 6865945581361480448. Fluxes are reported as peak flux over a 6 arcsec circular aperture centred on the detected MeerKAT position, and are corrected for the primary beam response. In the case of the flare, flux is measured in the 240 s image at the peak of the light curve.

	Stokes I, μJy	Stokes V, μJy	V/I
2021 June 20 (L2) full	70 ± 5	64 ± 5	92 per cent
2021 June 20 (L2) pre-flare	70 ± 9	58 ± 8	82 per cent
2021 June 20 (L2) flare	491 ± 36	425 ± 33	87 per cent
2021 June 20 (L2) post-flare	27 ± 8?		
2021 May 31 (L1)	14 ± 5		
2021 July 27 (L3)	28 ± 11		
2023 June 20 (L4)	16 ± 5		
2021 July 27 (U1)	10 ± 7		
2021 August 8 (U2)	39 ± 6		
2022 February 4 (U3)	15 ± 6		

Gaia DR3 6865945581361480448 is also noted in several other stellar catalogues using the VizieR catalogue access tool (Ochsenbein, Bauer & Marcout 2000), with astrometry, proper motion and spectrophotometric estimates that are in agreement with those obtained using *Gaia* (Monet et al. 2003; Zacharias et al. 2004; Fedorov, Akhmetov & Bobylev 2011; Girard et al. 2011). The star has a calculated distance of 1330^{+60}_{-80} pc placing it well within the Galaxy as a G type star ($T_{\rm eff} = 5300$ K; Babusiaux et al. 2023).

Having reprocessed the visibility data with the source excluded from the deconvolution mask, we are able to obtain a light curve for the source that is not mean-subtracted (as opposed to the normal TRON outputs, which yield mean-subtracted light curves). This is shown in Fig. 2, in units of apparent flux. The light curve shows a substantial flare between approximately 21:20 and 00:05 UTC, as well as detectable flux outside the flare.

The source being off-axis, the power beam in its direction will vary in time and frequency. We use the MeerKAT primary beam holography measurements of de Villiers (2023) to compute the expected power beam towards the source. The power beam gain as a function of time for the bottom (highest gain), mid, and top (lowest gain) of the band is also plotted in Fig. 2. The variation of the beam gain in time is not significant for our purposes, being within 2 per cent, 5 per cent, and 10 per cent at the bottom, middle, and top of the band, respectively. We adopt a mean value of 0.55 for the mid-*L*-band power beam gain (and 0.8 for UHF), and apply this value to derive the intrinsic fluxes quoted below. We also note that the instrumental leakage from Stokes I to Stokes V due to the primary beam is expected to be below 0.15 per cent as per the above measurements (not plotted).

The star manifests itself as a 70 ± 5 μJy continuum source in the deep 10 h image, which corresponds to the mean flux value across the light curve. The flare peaks at 491 ± 36 μJy. To get an estimate for the fluxes pre- and post-flare, we image those segments of the data separately, and fit a Gaussian component. The resulting flux estimates are summarized in Table 1. The source is reliably detected pre-flare in Stokes I and V. Post-flare, there is only a tentative detection in Stokes I (a 3.5σ peak, slightly offset from the source position, so we can not exclude the possibility of this being a noise excursion. This is indicated by a question mark in the table), and no detection in Stokes V. The source shows a very high circular polarization fraction of over 85 per cent both pre- and during the flare. We should note that, given the complex behaviour of the dynamic spectrum (discussed

below), these wideband flux measurements are crude at best. We do not detect any linear polarization component, neither in the wideband images, nor in the Stokes QU dynamic spectra, nor in the Faraday spectrum yielded by rotation measure synthesis.

With multiple observations of the field available as part of the PARROT follow-up (Smirnov et al. 2024), we are able to check if the source is detected in other epochs. None of them show a clear (over 4σ) detection (Fig. 3), however there is a hint of emission in the L4 and U2 epochs, just to the south-east of *Gaia* DR3 6865945581361480448. Its association with the star is uncertain, particularly in the UHF images, due to blending with nearby confusing sources. For all other epochs, we may take the peak flux at the source position to be an upper limit. The L2 image also contains a hint (23 μJy peak) of a compact source, designated 'B', just to the east of the star, which is also clearly visible in the 240 s Stokes V image. Any physical association is unlikely – the on-sky separation between source B and the star would correspond to a minimum physical distance of approximately 21 000 au – and the 'source' is almost certainly associated with a point spread function (PSF) sidelobe (bottom right image of Fig. 3) produced at the peak of the flare. Note that the star is excluded from the deconvolution mask in these images.

Using the $L2$ epoch observations, we construct a dynamic spectrum of the source, using the DYNSPECMS tool[2] (Callingham et al. 2021; Smirnov et al. 2024, 2025; Tasse et al. submitted). This is presented in Fig. 4, and shows evidence of drift across the passband of order $\sim$ 10 MHz min^{-1}.

In the *Gaia* DR3 release, this star is catalogued as having been observed 34 times between September 2014 and May 2017, with a mean G magnitude of 14.7883 ± 0.0021. The associated time-series shows clear evidence of consistent variability, with a $\Delta m\sim$ 0.11, and a Lomb–Scargle analysis yields a dominant period of 1.19 d. *Gaia* DR3 6865945581361480448 is coincident with star AP60750815 in the All Sky Automated Survey for SuperNovae (ASAS-SN) programme (Shappee et al. 2014; Kochanek et al. 2017), with a $m_V = 15.09 \pm 0.056$ over 198 epochs between May 2014 and September 2018, again showing a consistently variable albeit noisier time-series ($\Delta m\sim$ 0.3) from which a Lomb–Scargle analysis recovers the same 1.19 d period. The duration of MKT J200730.4−203549's L2 flare ($\sim$2 h), its high circular polarization and associated estimated brightness temperature ($>10^{12}$K), as derived from the luminosity estimates below, all point towards a coherent emission process. A supervised machine-learning based classification of 12.4 million variable sources in the *Gaia* DR3 catalogue flagged this source as a likely RS CVn variable (Rimoldini et al. 2023).

RS CVn binaries are chromospherically active on account of their tight, tidally locked, orbital orientation resulting in high rotational velocities and complex magnetic field topologies associated with prevalent star-spots on one or both of the component stars, which are typically of the F, G, or K spectral type. These conditions give rise to distinct emission properties observable at multiple passbands. The orbital period of such systems – ranging from $\sim$1 to $\sim$30 d – is easily detectable optically, with a magnitude variation typically of $\pm$0.2, and in certain viewing alignments, periodic eclipses are present. The rotationally enhanced magnetic activity manifests itself with the presence of strong Hα, Ca II, H, and K emission lines, with flare-like activity observed in both the EUV/X-ray and radio passbands when presumed magnetic loop reconnection events occur, with the resulting observed long duration ($\sim$ hours) and highly circularly polarized radio emission. Recent observations at low frequencies using LOFAR for 14 RS CVn systems suggest the source of this emission is one or both of the stellar chromospheres or via electrodynamic interactions between the stars (Toet et al. 2021).

Whilst RS CVn systems are known to produce both quiescent and enhanced ('flare') radio emission, the conventional understanding is that gyrosynchrotron processes dominate, yielding low levels of circularly polarized emission (Chiuderi Drago & Klein 1990). However, there have also been a number of cases reported in the literature where prolonged ($\sim$ hours) pronounced flare emission from such systems has been reported at GHz bands to be associated with consistently high levels (>40 per cent) of circular polarization associated with brightness temperatures $>10^{12}$ K with evidence of drift across the bandpasses ($\sim$1–10 MHz min^{-1}) that are difficult to explain without involving a coherent process, with several authors implicating the electron cyclotron maser instability (ECMI; Mutel et al. 1987; Osten et al. 2000; García-Sánchez, Paredes & Ribó 2003; Slee, Wilson & Ramsay).

Given the bandpass of 856 MHz and a central channel frequency of 1.284 GHz, one can estimate both peak and quiescent luminosity of $L_{\rm peak}\sim 1.04 \times 10^{18}$ erg s^{-1} Hz^{-1} and $L_{\rm q}\sim 1.49 \times 10^{17}$ erg s^{-1} Hz^{-1}. This compares favourably with RS CVn luminosities reported between 10^{16} and 10^{18} erg s^{-1} Hz^{-1} at this frequency band, with the latter being associated with 'superflare' activity having its origin in local coherent emission processes in the RS CVn system (Mutel et al. 1987).

The observational data we have to hand – periodicity of 1.19 d, consistent variability of $\sim\pm$ 0.2 magnitudes, and the physical properties of the observed flare – given its duration $\sim$2 h and high circular polarization fraction – are all consistent with *Gaia* DR3 6865945581361480448/MKT J200730.4−203550 being a distant RS CVn. The dynamic spectrum (Fig. 4) is of particular interest, as there is some suggestion of drifting across the 0.9–1.7 GHz bandpass similar to ECMI emission observed from the RS CVn binary HR 1099 at 1.384 GHz albeit with a smaller bandwidth of 104 MHz, again associated with $\sim$2 h highly circularly polarized flare events (Slee, Wilson & Ramsay 2008). An examination of the archived *Gaia* XP mean spectrum for 6865945581361480448 shows no evidence for emission lines, however this is not unexpected given its low spectral resolution and averaged nature – follow-up high-resolution spectroscopy would likely confirm the characteristic chromospheric emission-line signature.

4 CONCLUSIONS

MeerKAT has proven itself to be a remarkable instrument for the detection of faint, medium-time-scale radio transients and variables, and we can expect a systematic reprocessing of archival synthesis imaging data to yield many new discoveries. A reprocessing of the PARROT fields yielded a new transient, associated with the star *Gaia* DR3 6865945581361480448. The optical properties of the star are indicative of it being a distant RS CVn binary, and the observed radio behaviour (i.e. the nature of the dynamic spectrum, and the high degree of circular polarization) are consistent with an ECMI burst from such a system.

Unlike Letter I of this series, where the detections were made at the centre of the observed fields, and where the fields were already known to host variable sources, the detection reported on here is truly serendipitous, and underscores the value of the 'mining' approach. The detection was made far from the field centre, while the observation was done for unrelated reasons. This shows that the

[2]https://github.com/cyriltasse/DynSpecMS

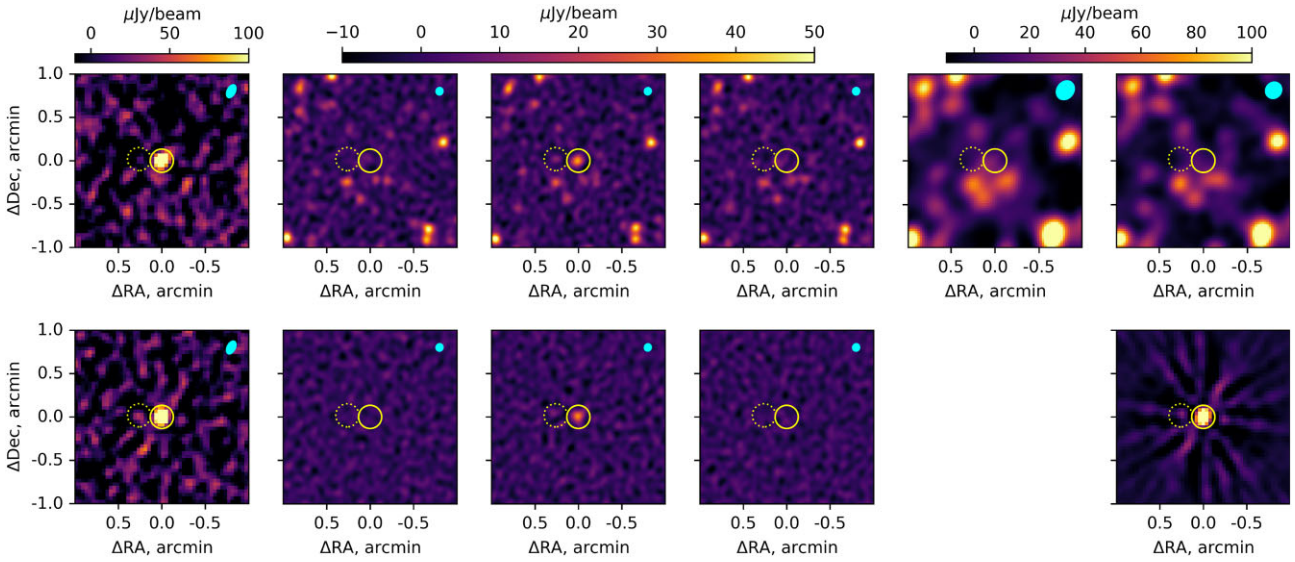

Figure 3. 2 arcmin × 2 arcmin image cutouts centred on *Gaia* DR3 6865945581361480448. Top row: Stokes *I*, bottom row: Stokes *V*. From left to right: (i) L2 epoch, 240 s image at peak of detection (not deconvolved); (ii–iv) deep *L*-band images for epochs *L*1, *L*2, and *L*4; (v, vi) deep UHF images for epochs U2 and U3 (Stokes *I* only). The bottom right image shows the PSF corresponding to the 240 s image at peak of detection. The position of *Gaia* DR3 6865945581361480448 is indicated by the solid circle; the dotted circle indicates 'source' B (see the text).

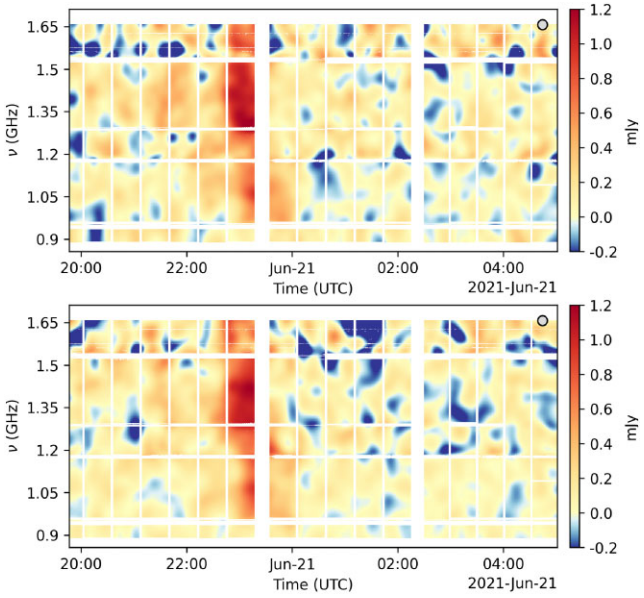

Figure 4. Primary beam corrected Stokes *I* (top) and *V* (bottom) dynamic spectra of *Gaia* DR3 6865945581361480448, smoothed to 35 MHz and 650 s (full width at half-maximum of the smoothing kernel is indicated in the top right). Gaps in the dynamic spectra correspond to calibrator scans and fully flagged (radio frequency interference contaminated) bands. Note that the noise across time and frequency is not uniform, due to (a) primary beam correction and (b) the frequency ranges between 0.9–1, 1.2–1.3, and 1.55–1.65 GHz having a larger flagged data fraction.

TRON pipeline is capable of discovering transients and variables of different astrophysical nature, over the entire field of view of the telescope.

DATA AVAILABILITY

The raw data underlying this article are publicly available via the SARAO archive,[3] under proposal ID SSV-20200715-SA-01.

ACKNOWLEDGEMENTS

The MeerKAT telescope is operated by the South African Radio Astronomy Observatory, which is a facility of the National Research Foundation, an agency of the Department of Science and Innovation. OMS's, JSK's, and VGGS's research was supported by the South African Research Chairs Initiative of the Department of Science and Technology and National Research Foundation (grant No. 81737). MAT gratefully acknowledges the support of the UK's Science & Technology Facilities Council (STFC) through grant awards ST/R000905/1 and ST/W00125X/1. We acknowledge the financial support of the Breakthrough Listen project. Breakthrough Listen is managed by the Breakthrough Initiatives, sponsored by the Breakthrough Prize Foundation.

REFERENCES

Babusiaux C. et al., 2023, A&A, 674, A32
Callingham J. R. et al., 2021, A&A, 648, A13
Chiuderi Drago F., Klein K. L., 1990, Ap&SS, 170, 81
de Villiers M. S., 2023, AJ, 165, 78
Fedorov P. N., Akhmetov V. S., Bobylev V. V., 2011, MNRAS, 416, 403
Gaia Collaboration, 2016, A&A, 595, A1
Gaia Collaboration, 2023, A&A, 674, A1
García-Sánchez J., Paredes J. M., Ribó M., 2003, A&A, 403, 613
Girard T. M. et al., 2011, AJ, 142, 15
Heywood I. et al., 2022, ApJ, 925, 165
Kochanek C. S. et al., 2017, PASP, 129, 104502
Monet D. G. et al., 2003, AJ, 125, 984
Mutel R. L., Morris D. H., Doiron D. J., Lestrade J. F., 1987, AJ, 93, 1220
Ochsenbein F., Bauer P., Marcout J., 2000, A&AS, 143, 23

[3] https://archive.sarao.ac.za

Osten R. A., Brown A., Ayres T. R., Linsky J. L., Drake S. A., Gagné M., Stern R. A., 2000, ApJ, 544, 953
Rimoldini L. et al., 2023, A&A, 674, A14
Shappee B. J. et al., 2014, ApJ, 788, 48
Slee O. B., Wilson W., Ramsay G., 2008, PASA, 25, 94
Smirnov O. M. et al., 2024, MNRAS, 528, 6517
Smirnov O. M. et al., 2025, MNRAS, 538, L62
Toet S. E. B., Vedantham H. K., Callingham J. R., Veken K. C., Shimwell T. W., Zarka P., Röttgering H. J. A., Drabent A., 2021, A&A, 654, A21
Zacharias N., Monet D. G., Levine S. E., Urban S. E., Gaume R., Wycoff G. L., 2004, in American Astronomical Society Meeting Abstracts, Vol. 205, p. 48.15

This paper has been typeset from a TEX/LATEX file prepared by the author.